Materials Science Forum Vol. 442 (2003) pp. 17-26
online at http://www.scientific.net

Analysis of Microstructure and Electrochemical Efficiency of Chill Cast Al-Zn-Mg Alloys Designed for Cathodic Protection Applications

J. Genesca[1], R. Herrera[2], C. Gonzalez[1], O. Alvarez[3] and J.A. Juarez-Islas[3]

[1]Fac. de Química-UNAM, Circuito Exterior S/N, Cd. Universitaria, 04510, México, D.F.

[2]Inst. de Física-UNAM, Circuito Exterior S/N, Cd. Universitaria, 04510, México, D.F.

[3]Inst. de Investigaciones en Materiales-UNAM, Circuito Exterior S/N, Cd. Universitaria, 04510, México, D.F.

Keywords: Al-Alloys, Electrochemical Efficiency, Microstructure, Sacrificial Anode, Solidification

Abstract.

This work carries out an analysis of the structure obtained in gravity chill cast Al-5.3 at. % Zn with additions of 5.3, 6.5, 7.5 and 11.5 at. % Mg. The as-cast microstructure consisted of α-Al dendrites, the intermetallic τ in α-Al solid solution and eutectic α+τ in interdendritic regions. The electrochemical behavior of alloys in both as-cast and heat treated ingots was investigated in 3% NaCl solution at room temperature. Results showed that the eutectic in interdendritic regions and the intermetallic in α-Al solid solution have an impact on the electrochemical efficiency of the alloys under study which are designed to be used as Al-sacrificial anodes. To correlate the effect of structure with electrochemical efficiency, it was analyzed the vertical section parallel to the Al-Mg side for a constant concentration of 5.3 at. % Zn together with growth temperature of phases obtained during solidification. Then, the range of solidification front velocities was predicted, where the α-Al and intermetallic τ phases grew simultaneously. These results, together with the predicted variation with growth velocity of solute concentration in the α-Al solid solution and the electrochemical efficiency values were used to select an alloy with an Al-5.34 at. % Zn-6.53 at. % Mg composition, which after heat treatment can be used as Al-sacrificial anode.

Introduction

The performance of Al-sacrificial anodes for cathodic protection applications has been directly related to its per cent of electrochemical efficiency or anode current capacity [1, 2]. Among the Al-alloys under study, the Al-Zn-Mg has been pointed out as a promising alloy system to be studied due to its low specific weight, low electrode potential and high current capacity [3]. During the development of Al-anodes some aspects have been considered to have an impact on their electrochemical behavior, such as structure [4],composition [5] and the effect of intermetallics in the α-Al matrix [6].

On the other hand, production of commercial Al-anodes involve the casting of Al-alloys into steel chill molds and during solidification a dendrite morphology develops with some interdendritic eutectic. To understand and to control the solidification process of the alloys, it is important to obtain its solidification path, which has been successfully done for binary alloys due to the availability of binary phase diagrams. For the Al-Zn-Mg system, two vertical sections are available in the literature [7] for constant concentrations of 1.69 and 5.3 at. % Zn. The vertical section with a constant concentration of 5.3 at. % Zn has been investigated during development of Al-anodes [3],

reporting the existence of an α-Al solid solution, the intermetallic τ with a composition corresponding to $Al_2Mg_3Zn_3$ [8, 9] and the eutectic α+τ. It has been pointed out [10] that growth temperatures, T_G, of competing constituents play a critical role in determining constitution and morphology of solidification microstructures. Growth temperatures (T_G) of dendrite, intermetallic and eutectic phases can be represented by equations of the form:

$$T_L - T_G = GD/V + BV^{0.5}, \text{ for dendrite [11]} \quad (1)$$

$$T_L - T_G = GD/V + B'V^{0.33}, \text{ for intermetallic [12]} \quad (2)$$

$$T_{Eu} - T_G = AV^{0.5}, \text{ for eutectic [13]} \quad (3)$$

where T_L and T_{Eu} are the equilibrium liquidus and eutectic temperatures, respectively, G the liquidus temperature gradient, D the liquidus diffusion coefficient in the liquid and V the solidification front velocity. The growth coefficients B, B′ and A are material constants that depend on operative interfacial energies and entrophies of fusion, liquid solute diffusivity and constitutional parameters [14] and being sometimes available in the literature [15,16]. Regarding dendritic solidification of the Al-Zn-Mg alloys, the model of Kurz et al. [17] was adopted for constrained dendrite growth at velocities up to the absolute stability limit in order to derive dendrite tip concentration in the melt, given by:

$$C^*_L = C_o/[1 - pIv(P)] \quad (4)$$

where C^*_L is the liquidus concentration in frot of the interface solidus/liquidus, C_o is the alloy compositioc, Iv(P) is the Ivantsov function, P (= VR/2D, with R being the dendritic tip radius) is the solute Peclet number and p (= 1- k) the complementary partition coefficient. The unknowns solute Peclet number and dendritic tip radius, R, are given by the solution of:

$$V^2A_1 + VB_2 + C = 0 \quad (5)$$

where $A_1 = \pi\Gamma/P^2D^2$, $B_2 = mC_op\xi_c/D[1 - pIv(P)]$ with $\xi_c = 1 - 2k/\{[1+(2\pi/P)]^{1/2} - 1 + 2k\}$ and C = G. Γ is the Gibbs-Thomson coefficient, m the liquidus slope and k the distribution coefficient.

This work reports experimental data obtained during and after solidification of Al-Zn alloys with Mg additions, in terms of growth temperature, microstructure and solute concentration. Growth temperature data is used to predict which of various alternative solidification microstructures is selected by competitive growth. Solute concentration data is compared with theoretical prediction and used to predict further precipitation of the intermetallic τ in α-Al solid solution after heat treatment. These data together with the electrochemical efficiency of heat treated ingots will help to select the alloy composition of Al-alloys to be used as Al-sacrificial anodes.

Experimental procedure

Al, Zn and Mg elements of commercial purity (99.5 %) were melted in a vacuum induction furnace under an argon protective atmosphere and gravity cast into steel molds of dimensions 75X75X500 mm. The alloy composition was chosen according to the vertical section parallel to the Al-Mg-Zn ternary diagram for a constant concentration of 5.3 at. % Zn, as shown in Fig. 1. The alloy composition of as-cast ingots was analyzed by plasma spectroscopy and is shown in Table 1.

Solidification history of the alloys was recorded using an Iotech Tempscan 1100 data acquisition system. Heat treatment of ingots was performed using a Thermoline furnace at 400 °C for 5 hr

under an argon atmosphere. Microstructure of ingots was revealed by electroetching the samples (25 V, -10°C), in a solution containing 10% perchloric acid in ethanol and observed under a Stereoscan 440 scanning electron microscope.

The electrochemical behavior of Al-alloys was investigated in 3% NaCl solution. The electrochemical tests were carried out in a three-electrode cell arrangement. The samples of the Al-anode were put in a sample holder presenting an exposing area of 125 mm^2 to the electrolyte. A platinum gauge was used as a counter electrode and a saturated calomel electrode was employed as a reference electrode.

Alloy	Zn	Mg	Si	Cu	Al
C_1	5.31	5.32	0.17	0.003	bal.
C_2	5.34	6.53	0.20	0.002	bal.
C_3	5.33	7.52	0.16	0.005	bal.
C_4	5.35	11.54	0.16	0.002	bal.

Table 1. Chemical composition of ingots (in at. %).

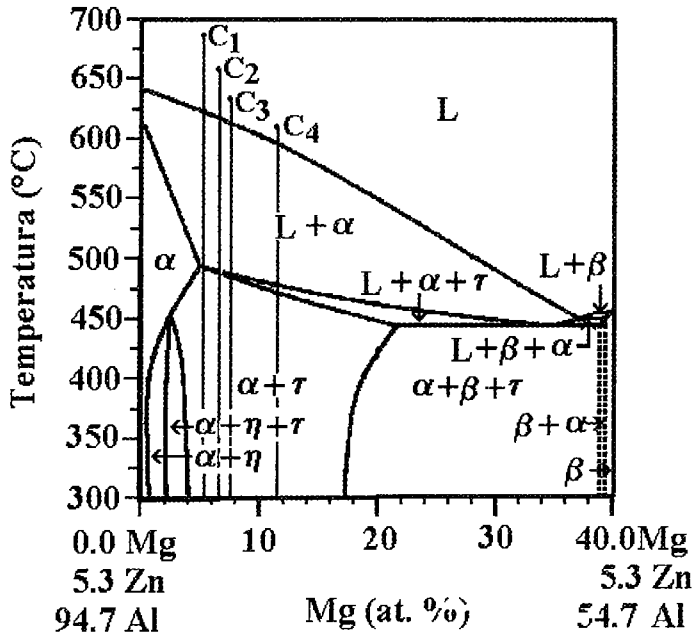

Fig. 1. Vertical section for a constant concentration of 5.3 at. % Zn of the ternary Al-Zn-Mg phase diagram. C_1, C_2, C_3 and C_4 represent the alloys under study.

Results

The microsconstituents observed in gravity chill-cast and heat treated ingots consisted mainly of α-Al dendrites, the intermetallic τ in α-Al solid solution and the eutectic α+τ in interdendritic regions (see Fig. 2). Quantitative metallography performed in as-cast and heat-treated ingots showed that

in α-Al solid solution was observed, reaching a maximum value of 5.5 vol. % when the Mg content was 6.5 at. % (see Table 2).

In agreement with Fig. 1, during solidification of Al-alloys in steel molds, α-Al was the first phase to grow which developed a dendrite pattern. As the solidification continued, the liquid surrounding the advancing solid/liquid interface was enriched with solute and as the temperature dropped and a phase transformation temperature was reached, phases such as the intermetallic τ grew. Fig. 3 shows the outcome of the thermocouples inserted in the liquid melt during solidification of Al-alloys in terms of plots of temperature versus time. The thermal arrest indicated in this figure resulted from the passage of the solidification front and thus indicated a growth temperature. The dendrite interface of α-Al is expected to be associated with a finite freezing range, so we took the temperature of initial departure (change in slope in Fig. 3) as indicative of α-Al tip temperature, $T_{G,\alpha}$, followed by growth temperatures of the intermetallic $T_{G,\tau}$ and the eutectic $T_{G,\alpha+\tau}$.

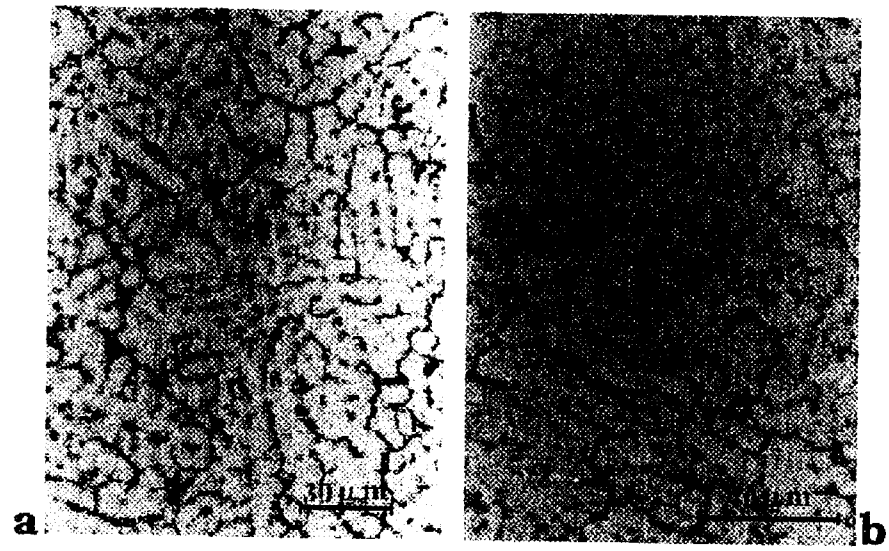

Fig. 2. A representative microstructure observed in (a) as-cast and (b) heat treated ingots.

Alloy	As-cast ingot			Heat treated ingot		
	α-Al	Eutectic α+τ	τ-Phase	α-Al	Eutectic α+τ	τ-Phase
C_1	89.3±2.3	10.0±0.43	0.70±0.04	89.30±2.3	10.0±0.43	0.70±0.04
C_2	86.5± 3.1	12.3±0.25	1.17±0.7	82.2± 1.5	12.3±0.25	5.50±0.07
C_3	83.0± 1.2	15.2±0.36	1.74±0.05	82.0±1.4	15.2±0.36	2.80±0.08
C_4	81.9±2.4	15.8±0.41	2.25±0.08	81.4±2.1	15.8±0.41	2.75±0.08

Table 2. Amount of eutectic and intermetallic detected in as-cast and heat treated ingots (in vol. %).

Table 3 shows equilibrium and growth temperatures taken from Fig. 1 and 3, respectively, for the α-Al, the intermetallic τ and the eutectic α+τ. These data together with a diffusion coefficient, $D=3X10^3$ $\mu m^2/s$ [18], a Gibbs-Thomson parameter, $\Gamma=0.0106$ Kμm [19], a liquidus slope value, m_L=-5.5 K/at. % (for region L+α) and -3.0 K/at. % (for region L+α+τ), with experimental values of liquidus temperature gradient, $G_L=5X10^{-4}$ K/μm and a solidification front velocity, V=~450 μm/s, were employed to derived the constants B and B´ for α-Al and the intermetallic τ, respectively, and

liquidus temperature gradient, G_L=5X10^{-4} K/μm and a solidification front velocity, V=~450 μm/s, were employed to derived the constants B and B′ for α-Al and the intermetallic τ, respectively, and are shown in Table 4. The value for the constant A (=0.0612 Ks$^{1/2}$/μm$^{-1/2}$) for the eutectic was between the values ranging from 0.023 to 0.128 Ksec$^{1/2}$/μm$^{-1/2}$ measured for the Al-Al_2Cu and Al-Zn eutectics [20,21].

Alloy	T_L (°C)	$T_{G,\alpha}$ (°C)	T_τ (°C)	$T_{G,\tau}$ (°C)	T_{Eu} (°C)	$T_{G,Eu}$ (°C)
C_1	622.9	620.0	491.8	490.0	442.6	441.2
C_2	615.7	613.3	490.0	488.5	442.6	441.3
C_3	613.1	610.5	488.5	486.6	442.6	441.3
C_4	596.7	594.0	477.0	475.0	442.6	441.4

Table 3. Liquidus and growth temperatures of α-Al, intermetallic τ and eutectic α+τ.

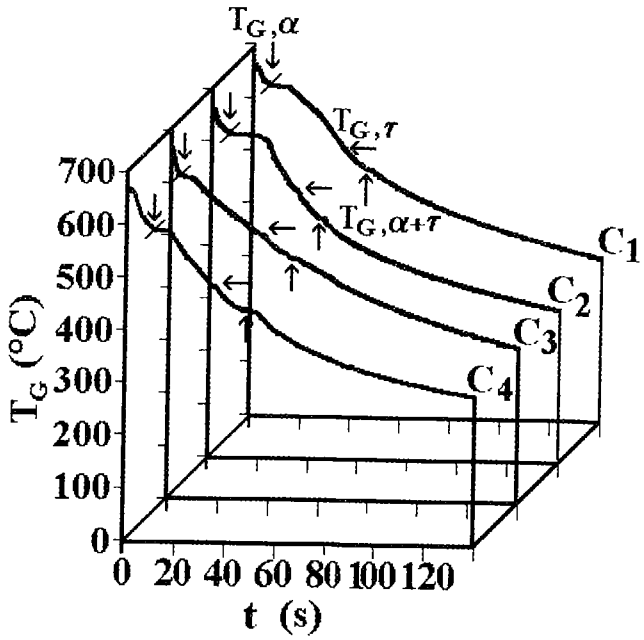

Fig. 3. Plots of temperature versus time for the alloys under study.

Alloy	Region L+α		Region L+α+τ	
	B (Ks$^{1/2}$/μm$^{-1/2}$)	B′ (Ks$^{1/2}$/μm$^{-1/2}$)	B (Ks$^{1/2}$/μm$^{-1/2}$)	B′ (Ks$^{1/2}$/μm$^{-1/2}$)
C_1	0.0590	0.1189	0.0263	0.1037
C_2	0.0591	0.1277	0.0277	0.1114
C_3	0.0648	0.1348	0.0289	0.1177
C_4	0.0741	0.1616	0.0331	0.1411

$B=[2\pi^2\Gamma m_L(k-1)/D]^{1/2}$ and $B'=[m_L C_o(k-1)]^{2/3}[\Gamma/D_L k]^{1/3}$

Table 4. Constants B for α-Al and B′ for intermetallic τ.

In particular, the constants B and B′ together with the liquidus temperatures for α-Al and intermetallic τ were fed into equations (1) and (2), respectively, to derive growth temperatures as a function of solidification front velocity only for region L+α+τ, and are plotted in Fig. 4. As can be observed, the α-Al and the intermetallic τ grew almost simultaneously in the range of solidification front velocities between 10^0 to $5X10^3$ μm/s. According to our experimental conditions, the solidification front velocity of 450 μm/s achieved during cooling of the Al-alloys was in the range of solidification front velocities where both phases growth simultaneously.

Regarding distribution of solute during dendrite solidification of Al-Zn-Mg alloys, Fig. 5 shows predictions for solute concentration C^*_s and C^*_L as a function of solidification front velocity for the alloys under study according to equation (4), for region L+α+τ. As can be observed, the amount of solute increased as the solidification front velocity increased and will be approximately equal to C_o when the solidification front velocity reaches the absolute stability value [22].

In addition, Table 5 shows the amount of solute concentration (Zn+Mg) retained in solid solution, C^*_s, for a solidification front velocity of 450 μm/s predicted according to equation (4). Table 5 also includes values obtained by WDS-microanalysis performed in the alloys under study. As can be observed, experimental values are between predicted values.

Alloy	Prediction (at. % Zn+Mg)	WDX-microanalysis (at. % Zn+Mg)
C1	8.3	7.5 to 9.2
C2	10.2	9.4 to 11.3
C3	11.3	10.2 to 12.2
C4	13.2	12.3 to 14.2

Table 5. Zn + Mg retained in α-Al solid solution according to predictions and WDS microanalysis

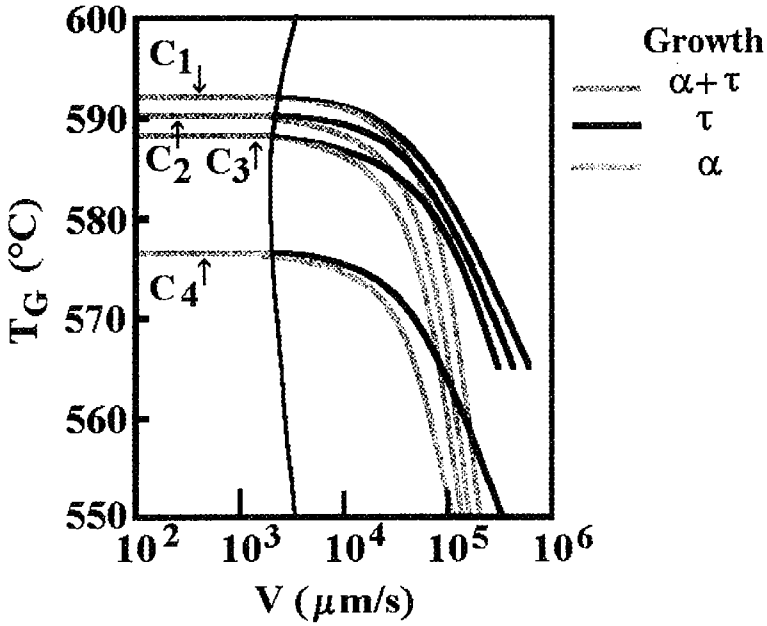

Fig. 4. Competitive growth analysis for the α-Al and τ-intermetallic of region L+α+τ.

Alloys in the as-cast and heat treated conditions were electrochemically evaluated. The as-cast

alloy with a solute concentration of Zn+Mg close to the maximum concentration of solute at equilibrium (10.8 at. %), showed an electrochemical efficiency value of 68%, while alloys with a high concentration of Zn+Mg reached electrochemical efficiency values up to 78%, as shown in Table 6. The same table shows electrochemical efficiency values of heat treated ingots (400°C, 5 hr). Alloys with a solute concentration close to the maximum concentration of solute at equilibrium showed almost the same value of electrochemical efficiency, while the alloy with Zn+Mg content of 11.8 at. % reached an electrochemical efficiency value of 87%. This value decreased when the alloy content increased.

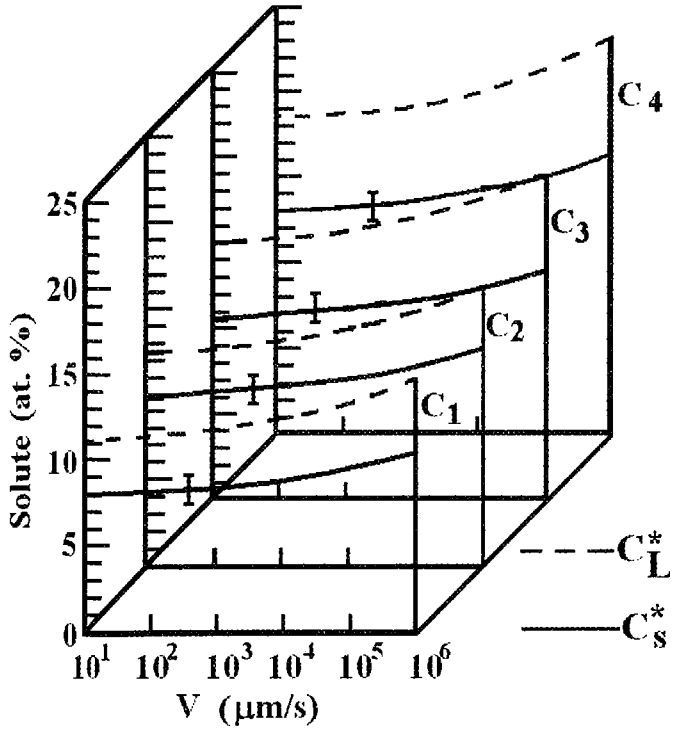

Fig. 5. Distribution of solute C^*_L and C^*_s according to eq. (4) together with experimental values.

Alloy	as-cast ingots (%)	heat treated ingots (%)
C1	68.3	69.1
C2	73.2	87.2
C3	78.2	86.4
C4	77.8	86.2

Table 6. Electrochemical efficiency of as-cast and heat treated ingots

Discussion

Microscopic observations carried out on gravity chill cast Al-alloys showed that the structure observed in as-cast ingots was of the equiaxed dendrite type with eutectic in interdendritic regions and even after heat treatment at 400°C for 5 hours, this structure still observed. Salinas et al. [4]

reported that the electrochemical efficiency varied between Al-Zn alloys with a constant concentration of Zn but with columnar or equiaxed dendrites. The alloys with the best electrochemical efficiency were those with an equiaxed dendrite structure showing electrochemical efficiencies of 68%. As reported above, the as-cast alloys under study showed a maximum value of electrochemical efficiency of 78.2%. This value was attributed to the presence of equiaxed dendrite structures and τ-phase in the α-Al solid solution. Regarding the presence of eutectic in interdendritic region, it was observed that it has a negative effect on the electrochemical efficiency as its volume per cent increased (see Fig. 6) because the eutectic is an stable constituent that did not dissolve during the electrochemical test.

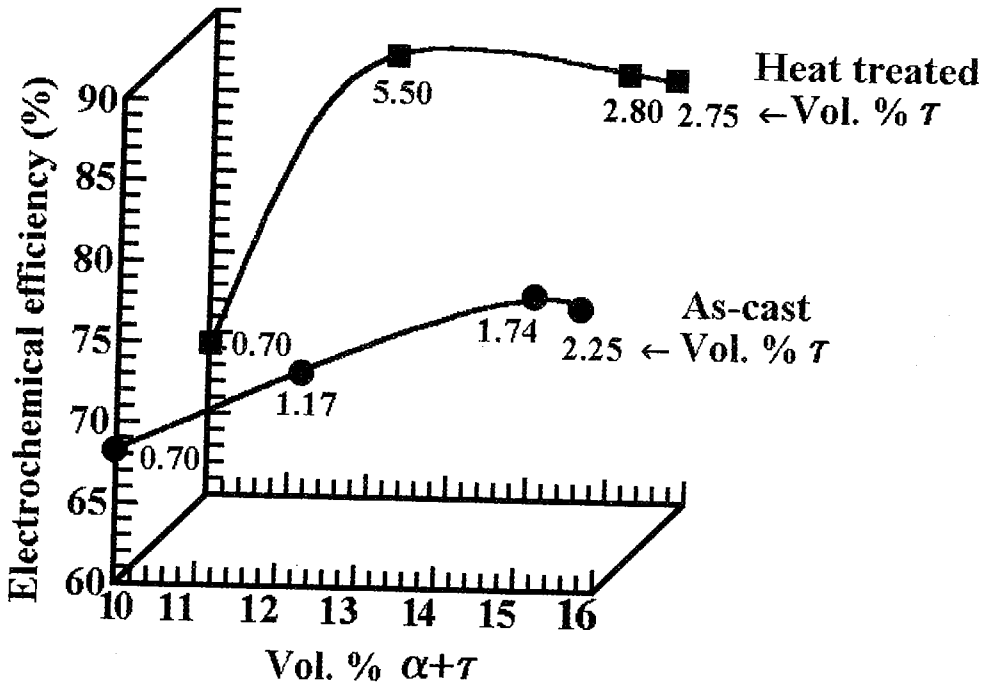

Fig. 6. Electrochemical efficiency as a function of amount of eutectic and intermetallic τ.

On the other hand, Barbucci et al.[7] reported that after heat treatment (400°C) of Al-Zn-Mg alloys, the electrochemical efficiency reached a maximum value of 81 %. This increase was attributed to a further precipitation of the intermetallic τ in the α-Al solid solution. In this work, after heat treatment of as-cast ingots at 400°C for 5 hours, the intermetallic τ reached a maximum value of 5.5 vol. % showing an encouraging electrochemical efficiency value of 87.2 % in an Al-alloy with 5.3 at. % Zn + 6.5 at. % Mg.

Monitoring the solidification path of the Al-alloys under study allowed us to know the growth temperatures of competing constituents which played a critical role in determining cathodic properties of as-cast ingots. It was found by competitive growth analysis that solidification front velocities of 450 μm/s achieved during the experiments were high enough to permit the simultaneous growth of the α and τ phases when the solidification path reached the L+α+τ region.

The model for constrained dendrite growth [17] at velocities up to the absolute stability limit was adopted during dendrite solidification to derive solute concentration in the melt. Predictions of solute concentration for region L+α+τ were close to those determined experimentally, as shown in

Table 5. This knowledge of the amount of solute in solid solution was used to derive the fraction of precipitates that form during aging according to:

$$\Delta f_p = k_1[C_m - C^o_m]^3 \quad \text{Ref. [18]} \tag{7}$$

where $k_1 = 0.1399$, C_m the mean solute concentration in the matrix and C^o_m the matrix solute content in stabilized base material. According to equation (7) the maximum fraction of precipitates for the alloys under study after aging will be ~ 5.94 vol. % which is close to the value of 5.5 vol. % obtained experimentally. Promoting the precipitation of the intermetallic τ-$Al_2Mg_3Zn_3$ or τ in the α-Al solid solution will improve its electrochemical properties avoiding the formation of the continuous, adherent and protective oxide film on the Al-anode.

Summary

1.- As-cast Al-Zn-Mg alloys showed a microstructure which consisted of α-Al dendrites and the eutectic $\alpha + \tau$ in interdendritic regions.
2.- The thermal analysis performed in the alloys under study indicated the temperature changes in the alloy as it cools through phase transformation intervals, giving growth temperatures for the α-phase, the intermetallic τ and the eutectic $\alpha + \tau$.
3.- The competitive growth analysis performed in Al-alloys showed that when solidification of the liquid melt reached the L+α+τ region, α and τ phases grew simultaneously up to solidification from velocities close to $5X10^3$ μm/s.
4.- Predictions for C_S* and C^*_L as a function of solidification front velocity carried out in region L+α+τ, showed values similar to those obtained experimentally.
5.- The amount of solute in solid solution was used to derive the amount of precipitates which form after aging giving a value of 5.94 vol. %, close to the value achieved after heat treatment of ingots which was 5.5 vol. %.
6.- Heat treated Al-5.3 at. % Zn-6.5 at. % Mg alloy, with a volume fraction of the intermetallic τ in the α-Al solid solution of 0.055 showed an electrochemical efficiency of 87.2 %.

Acknowledgments

The authors acknowledge the financial support from DGAPA with grant IN102601 and CONACYT with grant NC-204. We also thank Mr. Caballero for carrying out the photographic work.

References

[1] J. A. Juarez-Islas and J. Genesca: Contribution to Science Vol. 1 (2001), p. 331.
[2] S. Valdes, B. Mena J. Genesca and J. A. Juarez-Islas: Mat. Eng. and Performance Vol. 10 (2001), p. 596.
[3] G. Bruzzone, A Barbucci and G Cerisola: Alloys and Compounds Vol. 247 (1997), p. 210.
[4] D. R. Salinas, S. G. Garcia and J. B. Bessone: Appl. Electrochemical Vol. 29 (1999), p. 1063.
[5] I. Gurrappa: Corrosion Prevention & Control June (1997), p. 69.
[6] A Barbucci, G. Cerisola, G. Bruzzone and A. Saccone: Electrochemical Acta, Vol. 42 (1997), p. 2369.

[7] G. M. Kuznetsov, A. D. Barsukov, G. B. Krivosheeva, E. V. Bashahksian: Izv. Vyss. Uchebn. Zaved. Tsvent. Metall. Vol. 2 (1985), p. 91.
[8] D. A. Petrov: *Ternary Alloys*, Vol. 3, ed. G. Petzow and G. E. Effemberg (VCH Weinheim, Germany, 1986), p. 57.
[9] A. K. Mukhopadhyay, Q. B. Yang and S. R. Singh: Acta Metall. Mater. Vol. 42 (1994), p. 3083.
[10] R. Trivedi and W. Kurz W: Int. Mat. Review Vol 39 (1994), p. 49.
[11] W. Kurz: Z. Metallkunde Vol. 69 (1978), p. 433.
[12] J. Hunt and S. Z. Lu.: Met. and Mat. Transactions A Vol 27A (1996), p. 611.
[13] J. A. Juarez-Islas and H. Jones: The Institute of Metals Vol 421 (1988), p. 492.
[14] A. J. Hernandez and H. Jones: Metall. Mater. Transactions A Vol 31A (2000), p. 327.
[15] D. M. Stefanescu: ISIJ International Vol. 35(6) (1995), p. 637.
[16] H. Jones: ISIJ International Vol. 35(6) (1995), p. 751.
[17] W. Kurz, B. Giovanola and R. Trivedi: Acta Metallurgica Vol. 34 (5) (1986), p. 823.
[18] B. J. Bjorneklett, O. Grong, O. R. Myhr and A. O. Klñuken: Metall. Mater. Transactions, Vol 30A (1999), p. 2667.
[19] G. Eger: Int. Z. Metallography Vol 4 (1993), p. 50.
[20] A. Moore and R. Elliot: The Solidificaction of Metals (The Iron and Steel Institute, London, 1968), p. 167.
[21] M. Tasa and J. D. Hunt: J. Cryst. Growth Vol. 34 (1976), p. 38.
[22] J.A. Juarez-Islas: J. of Materials Science Vol. 26 (1994), p. 5004.